Chemical trend of band offsets at wurtzite/zinc-blende heterocrystalline semiconductor interfaces

M. Murayama and T. Nakayama
Department of Physics, Faculty of Science, Chiba University, Yayoi Inage, Chiba 263, Japan
(Received 15 June 1993; revised manuscript received 22 October 1993)

The band structures of various semiconductors in both wurtzite (WZ) and zinc-blende (ZB) structures are calculated using the first-principles pseudopotential method within the local-density approximation, and then the band offsets at (111) WZ/ZB interfaces are evaluated for the band-edge states around fundamental gaps. We found that the band offsets are larger for "zone-boundary states" having large wave numbers perpendicular to [111] than for "zone-center states" having small wave numbers perpendicular to [111]. These phenomena occur because the former offsets are caused by the phase matching of a wave function through the first-nearest-neighboring site, whereas the latter are caused by the difference between the position of the third-nearest-neighboring site in the WZ and ZB structures. In addition, we show that the band offset increases with decreasing ionicity of the constituent semiconductor material, i.e., the magnitude of the band offset is determined by the competition between ionicity and covalency.

I. INTRODUCTION

Numerous theoretical and experimental studies of semiconductor heterosystems have been carried out, with subsequent results elucidating their physics.[1] This research has generally been focused on heteromaterial systems such as GaAs/AlAs. Here, however, we examine heterocrystalline (homomaterial) semiconductor systems of wurtzite (WZ)/zinc blende (ZB). One fundamental problem of this system concerns how different crystal structures affect its electronic structure. Our previous calculations of electronic structures of WZ/ZB superlattices of Si and ZnS (Refs. 2 and 3) showed that the electron and hole states both display a quantum-well-like localization in either the WZ or ZB layer, similar to ordinary superlattice systems such as GaAs/AlAs, and that the band offsets can be used to effectively characterize their structures. In the present paper, we calculate the band offsets at WZ/ZB interfaces of various semiconductors using the first-principles method based on density-functional theory, then clarify which mechanism produces the band offset, and how it changes in various semiconductors.

WZ and ZB are typical crystal structures of semiconductors. For most natural semiconductors, a variety of crystal forms exist which simultaneously possess both structures, briefly described as follows. (1) The Si and Ge crystals often have stacking faults[4,5] containing WZ/ZB interfaces between hexagonal (WZ) and cubic (ZB) diamond structures. These stacking faults appear during growth, and are dependent on the cooling process and concentration of impurities. Although such crystalline faults are often terminated with dislocations, their size is large enough, i.e., 0.01–0.1 μm, to show a definite WZ/ZB interface. (2) SiC, ZnS, and CdS also show many polytypes[6–8] consisting of periodically arranged WZ and ZB layers along the [111] direction; hence we consider them natural WZ/ZB superlattices. (3) Finally, single crystals of a needletype shape such as ZnS sometimes show stacking faults and twinning,[9] with WZ/ZB interfaces being present along the needle direction. On the other hand, for artificially produced semiconductors, (1) Koguchi *et al.*[10] recently succeeded in growing GaAs and InAs [111] whiskers on a GaAs substrate using a modern crystal-growth technique employing organometallic vapor phase epitaxy. These whiskers have a diameter of 20–100 nm, a length of 1–5 μm, and layered structures along the [111] direction comprised of WZ and ZB crystals. The origin of the layered structures has not been clarified, though it has been suggested that controlling the volume ratio of WZ and ZB, by changing growth conditions such as substrate temperature and material gas pressure, may lead to producing WZ/ZB superlattices made of various semiconductors. (2) Another recent crystal-growth technique has made it possible to epitaxialize semiconductors having a crystal structure that does not exist in nature,[11,12] e.g., GaN grown on a GaAs substrate,[13] in which GaN changes its crystal structure from WZ to ZB due to the existence of the substrate. With regard to all this research, the present study improves our understanding of electronic structures.

The band offset is an essential quantity characterizing heterointerfaces, being defined as a difference in energy between the band eigenenergy states of constituents at an interface, and sometimes called a band discontinuity. There are a number of theories[14–19] predicting band offsets, most of which consider them to be determined by the difference of energy levels between corresponding states of the interface constituents, and by the dipole potential at the interface.[20–22] The dipole potential is often caused by the charge transfer at the interface, and is generally considered to be a result of "matching the reference levels." However, previous calculations to determine the electronic structures of WZ/ZB systems of Si (Refs. 2 and 23) and ZnS (Refs. 2 and 3) showed that there is little charge transfer between the WZ and ZB layers, and therefore no dipole potential at their interface. If true, the band offset at the WZ/ZB interface would be determined only by the difference between original energy levels in WZ and ZB. Based on this, here we derive the

0163-1829/94/49(7)/4710(15)/$06.00

band offset by calculating separate versus system band structures.

Although several theoretical studies have compared the electronic structures of WZ and ZB,[24–27] and considered the electronic structures of WZ/ZB systems,[23,28–32] most examined only individual materials. Birman[24] was the first to compare energy bands of WZ and ZB by the tight-binding method, and pointed out that WZ states along [111] can be obtained by perturbing corresponding ZB states. Salehpour and Satpathy[25] calculated band structures of hexagonal (WZ) and cubic (ZB) diamond using the local-density approximation (LDA) and linear-muffin-tin-orbital method, and found significant differences in the character and value of the band gap, i.e., an indirect gap from Γ_{5v}^{+} to K_{2c} with 4.5 eV in WZ, versus an indirect gap from Γ_{25v}' to Δ_{1c} with 5.6 eV in ZB. Stacking faults in Si,[23,28–30] and polytypes[31,32] such as ZnS and SiC, are believed to be the only WZ/ZB systems previously studied. Chou, Cohen, and Louie[23] calculated the stacking fault energy and electronic structures of [111] stacking-fault systems in Si by the *ab initio* pseudopotential method under the LDA, and found defect states 0.1 eV above the top of the valence band to be consistent with a photoluminescence experiment. These results led to the present paper, which considers various heterocrystalline semiconductor systems of WZ and ZB in order to elucidate common characteristics and intrinsic features between materials.

In Sec. II, the crystal structures of WZ and ZB are described, as is the correspondence between their symmetry points in the Brillouin zone. Our calculational method is then presented for determining the electronic structure. Next, calculated results of the WZ and ZB band structures of various semiconductors are compared in Sec. III, and characteristics evident in both band structures are discussed. Section IV gives the band offsets for states around fundamental gaps, and is followed by an analysis of their origin and a prediction of their chemical trend using the sp^3-tight-binding method. In addition, brief remarks are provided in Sec. V concerning the structural stability of WZ and ZB, while Sec. VI is devoted to summarizing our findings.

II. CALCULATIONAL METHOD

A. Geometry

WZ/ZB systems can be produced by stacking WZ on ZB layers along the [111] direction.[2] We assume no strain at WZ/ZB interfaces, as was shown by Chou, Cohen, and Louie[23] for Si, and also an ideal structure for WZ layers.[2] Therefore, the lattice constants are the only parameters of concern for these crystal structures. Table I summarizes the lattice constants of materials used in our calculation, all of which were experimentally obtained.[33,34] For a material having only an experimentally determined lattice constant for the ZB structure, we use this lattice constant for the WZ structure as well, and vice versa. Although we consider the above-mentioned WZ/ZB systems, their electronic structures are not calculated as explained in Sec. II B. Instead, we calculate only the band structures of WZ and ZB, and then derive their band offset.

TABLE I. Lattice constants (a.u.) of various semiconductors used in the present calculation. All values are from Refs. 33 and 34.

IV family					
C	6.7299				
Si	10.2450				
SiC	8.2257				
III-V compounds					
AlN	8.2985	GaN	8.4580		
AlP	10.3150	GaP	10.2850	InP	11.0717
AlAs	10.6790	GaAs	10.6660	InAs	11.4300
AlSb	11.5770	GaSb	11.5000	InSb	12.2245
II-VI compounds					
ZnS	10.2080	CdS	10.9910	HgS	11.0400
ZnSe	10.6940	CdSe	11.4200	HgSe	11.4790
ZnTe	11.5090	CdTe	12.2280	HgTe	12.1910

Following this, the correspondence of the wave-number vectors between WZ and ZB is considered, being necessary to define the band offset between their corresponding states. The fcc and hexagonal Brillouin zones of the ZB and WZ structures, respectively, are shown in Figs. 1(a) and 1(b). When we compare two band structures whose Brillouin zones have different shapes, a reasonable approach is to establish a correspondence between states having the same wave-number vectors.[24–27] Such correspondence is acceptable for free-electron-like states, and is easily realized when the unit cell of ZB is twice as large along the [111] direction as the usual fcc unit cell,[24–27] i.e., the volume of the ZB Brillouin zone becomes the same as that of WZ, as shown in Fig. 1(a), and the number of ZB valence bands coincides with that of WZ. This approach was employed to compare the band structures of WZ and ZB for a tight-binding model semiconductor (Birman[24]); for CdSe, CdS, and ZnS (Bergstresser and Cohen[27]); and for diamond (Salehpour and Satpathy[25]). As examples, one of the four nonequivalent L points in the usual fcc Brillouin zone is folded into the Γ point in the half-size Brillouin zone [Fig. 1(a)], which we call the ΓL^{ZB} point, while the other L points and all X points are folded into points which we call LX^{ZB} points. These ΓL^{ZB} and LX^{ZB} points, respectively, have the same wave numbers as the Γ^{WZ} and U^{WZ} points, where the position of the U^{WZ} point located on the L^{WZ}-M^{WZ} line [Fig. 1(b)] is defined with the ratio L^{WZ}-U^{WZ}/U^{WZ}-$M^{WZ}=\frac{1}{2}$. In order to avoid complexity, we sometimes add the superscripts WZ and ZB to the symmetry points.

Another approach, however, is to use the same unit cell and thus the same Brillouin zone for both structures, which is possible, for example, when the unit cells are three times as large as the above-mentioned unit cells of WZ and ZB along [111]. The correspondence based on this approach is mathematically valid because the Hilbert space associated with each Bloch wave-number vector

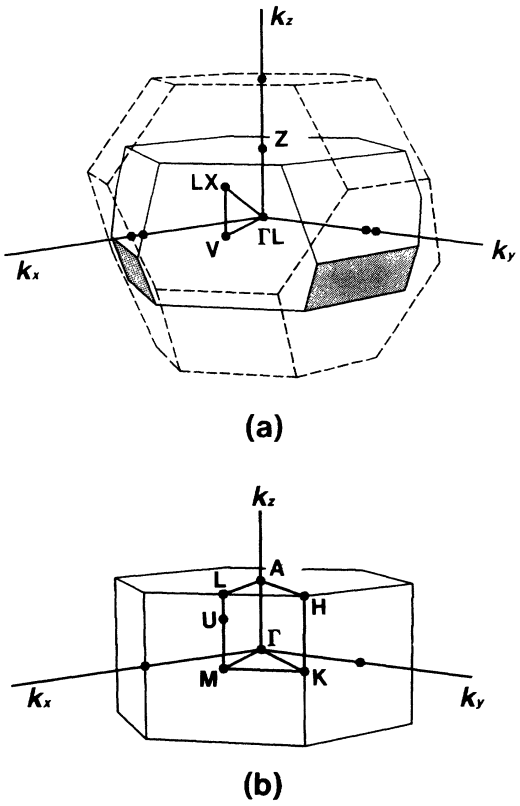

FIG. 1. Brillouin zones for (a) ZB and (b) WZ structures. Both Brillouin zones are drawn in the same scale and viewed from the same point, where the k_z axis is parallel to the [111] direction. In (a), the broken line indicates the familiar fcc Brillouin zone, the solid line that of the $\frac{1}{2}$ Brillouin zone corresponding to the double unit cell along the [111] direction. V is located at the center of the front surface of the $\frac{1}{2}$ Brillouin zone, and LX is located at the center of the hexagon of the fcc Brillouin zone, whose position is inside of the $\frac{1}{2}$ Brillouin zone and just above V along the [111] direction. The shaded planes indicate the surface common to both Brillouin zones. In (b), U divides the L-M line at a 1:2 ratio.

coincides with each other between WZ and ZB. In this case, the correspondence between states at symmetry points in ZB and WZ in Figs. 1(a) and 1(b) equals the correspondence between groups of points. Examples of this are

$$\left.\begin{array}{r}\text{point:}[0,0,\frac{1}{3}]\\ \Gamma^{\text{WZ}}\text{:}[0,0,0]\\ \text{point:}[0,0,-\frac{1}{3}]\end{array}\right\} \Longleftrightarrow \left\{\begin{array}{l}\text{point:}[0,0,\frac{1}{3}]\\ \Gamma L^{\text{ZB}}\text{:}[0,0,0]\\ \text{point:}[0,0,-\frac{1}{3}]\ ,\end{array}\right. \quad (1)$$

$$\left.\begin{array}{r}U_1^{\text{WZ}}\text{:}[\frac{1}{2},\frac{1}{2},\frac{1}{3}]\\ M^{\text{WZ}}\text{:}[\frac{1}{2},\frac{1}{2},0]\\ U_2^{\text{WZ}}\text{:}[\frac{1}{2},\frac{1}{2},-\frac{1}{3}]\end{array}\right\} \Longleftrightarrow \left\{\begin{array}{l}LX^{\text{ZB}}\text{:}[\frac{1}{2},\frac{1}{2},0]\\ V_2^{\text{ZB}}\text{:}[\frac{1}{2},\frac{1}{2},-\frac{1}{3}]\\ V_1^{\text{ZB}}\text{:}[\frac{1}{2},\frac{1}{2},\frac{1}{3}]\ ,\end{array}\right. \quad (2)$$

where we denote the points using a coordinate based on each reciprocal-lattice vector of WZ and ZB.[2]

B. Method

We employed the *ab initio* pseudopotential total-energy method within the LDA under density-functional theory,[35,36] using the *ab initio* pseudopotentials constructed by Bachelet, Hamann, and Schlüter.[37] For the exchange-correlation potential, we adopted the density-functional form of Ceperly and Alder[38] as parameterized by Perdew and Zunger.[39] The spin-orbit interaction is not included. These calculational methods are conventionally applied, and their details are described elsewhere.[2] Table II summarizes the applied primary parameters, where the energy cutoff is the maximum energy of a plane wave used in the expansion of the wave function.[40,41] When quantities such as the charge density are integrated over the Brillouin zone, we adopt the special point method,[42] with the number of k points in a full Brillouin zone being given. When the charge density is Fourier transformed from real to momentum space, we divide the unit cell into mesh points, the number of which is also given. It should be mentioned that the parameters shown in Table II are large enough to estimate the band offsets for C to CdSe, whereas for total energy we must utilize a large energy cutoff and fine mesh points to obtain precise results, i.e., the difference in the total energy between WZ and ZB structures is extremely small.[43] The calculational errors using these parameters are estimated to be ± 1 meV for an eigenvalue of the band state, thus applying to the band offset, and ± 5 meV/atom for total energies. The test of our calculation is presented in Sec. III, and compared with previous calculations.

The method we employed for calculating band offsets under the LDA band-structure scheme is also familiar,[20–22] and described elsewhere.[2,20] In this method, we calculate the band structures of both bulk crystals (WZ and ZB) and the corresponding WZ/ZB system. By calculating the bulk values, the energies of the associated band-edge states relative to the respective average potentials are obtained, while for WZ/ZB system the difference is evaluated between the average potential at the far right and left of the WZ/ZB interface. The sum of both contributions is considered to represent the band offset for that state. However, in previous calculations of WZ/ZB systems of Si (Refs. 2 and 23) and ZnS,[2,3] it was shown

TABLE II. Technical parameters for various semiconductors used in the present band-offset and total-energy calculations.

Material	Energy cutoff (Ry)	Number of k points	Number of mesh points in a unit cell
C(WZ)	62.41	324	24×24×38
C(ZB)	62.41	324	24×24×48
Si	16.00	324	16×16×32
SiC	42.25	324	22×22×44
AlN	41.34	324	22×22×44
AlAs	16.00	768	16×16×32
GaN	39.81	324	22×22×44
GaAs	16.00	768	16×16×32
CdS	16.00	324	20×20×40
CdSe	16.00	324	20×20×40
Others	14.44	96	16×16×32

that the charge transfer through WZ/ZB interfaces is extremely small, and no dipole potential appears at the interface. Furthermore, because the filling ratio of atoms are identical in WZ and ZB, the difference of the average potential is less than 1 meV. Therefore, this enables the band offset to be evaluated using only the calculated band structure of the bulk values of WZ and ZB. To evaluate the band structures of WZ/ZB systems comprised of other semiconductors, we assume no difference is present between the average potential at the WZ/ZB interfaces; hence we calculate only the band structures of bulk crystals. This assumption is consistent with the calculated results in Sec. IV, that show Si and ZnS are representative materials among various semiconductors having small and large values of ionicity, respectively.

Finally, we note that the band-structure calculation under the LDA underestimates the band-gap energies of semiconductors.[44,45] Moreover, the use of the LDA Kohn-Sham eigenvalues for band offsets presents problems.[46,47] In fact, from the calculated results for accurate quasiparticle energies,[44,45] corrections to the LDA shift its energy spectra depending on the material and state, this being physically caused by a discontinuity in the exchange-correlation potential upon addition of an electron.[48,49] Such corrections are therefore important when calculating the band offset. A typical example of this is shown in the Schottky-barrier heights calculations at metal/semiconductor interfaces.[50,51] Since we do not correct these energies here, but consider only the electronic structures within the LDA, exact values of band offsets cannot be obtained. On the other hand, the detailed investigation by Godby, Schlüter, and Sham[45] of the quasiparticle nonlocal self-energy operator showed that the range of the self-energy operator is about 5 a.u. or less for the component semiconductors. For the WZ/ZB system, the WZ and ZB layers consist of the same material, and their local atomic configuration is the same within about 7 a.u. (see Table VI); hence we believe that the corrections to the corresponding LDA energy levels in WZ and ZB are similar, and also that the presented chemical trends of the LDA band offset hold.

III. BAND STRUCTURES OF ZB AND WZ STRUCTURES

Because the topology of band structures are similar among various semiconductors, the calculated band structures of ZB and WZ for GaAs are presented as a typical example in Figs. 2(a) and 2(b). Tables III and IV, respectively, summarize the energies of representative states at symmetry points for various semiconductors with ZB and WZ structures. All the energies are measured from the top of the valence band: the heavy-hole states (Γ_{15v} for ZB and Γ_{6v} for WZ). The representations follow the notations by Bergstresser and Cohen,[27] where the conduction- (valence-) band state has the subscript c (v), and the values in parentheses indicate the degeneracy of the energy level.

To verify these calculated results, we compared them with previous calculations. Numerous LDA calculations are available regarding the electronic structures of ZB of various semiconductors, and from among them we selected Si and ZnTe. Yin and Cohen[41] calculated the structural properties of Si using the *ab initio* pseudopotential method under the LDA. Eigenvalues relative to the valence-band maximum by their and our calculations are, respectively, -11.93 and -11.96 (Γ_{1v}), 2.53 and

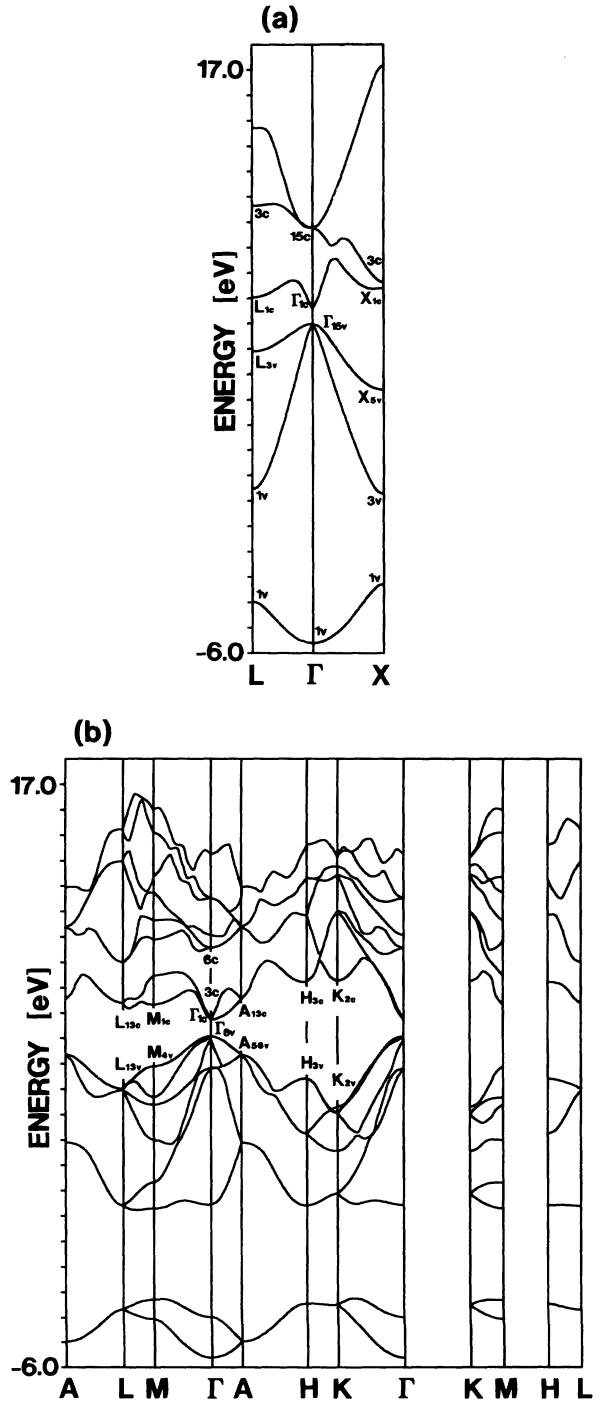

FIG. 2. Calculated band structures of GaAs in (a) ZB and (b) WZ structures. The band structure of ZB is shown in a familiar fcc Brillouin zone. The scales of the horizontal axis correspond, respectively.

2.56 (Γ_{15c}), 3.29 and 3.31 (Γ_{1c}), −7.78 and −7.81 (X_{1v}), −2.88 and −2.85 (X_{5v}), 0.61 and 0.63 (X_{1c}), −9.52 and −9.61 (L_{1v}), −7.00 and −6.98 (L_{1v}), −1.20 and −1.19 (L_{3v}), 1.48 and 1.51 (L_{1c}), and 3.31 and 3.33 (L_{3c}) eV, where good agreement is obviously present. Wei and Zunger[52] calculated the electronic structure of ZnTe using the full linear augmented-plane-wave (FLAPW) method under the LDA. Eigenvalues by them are −11.06 (Γ_{1v}), 2.01 (Γ_{1c}), 4.15 (Γ_{15c}), −9.71 (X_{1v}), −5.10 (X_{3v}), −2.26 (X_{5v}), 2.08 (X_{1c}), 2.20 (X_{3c}), −10.16 (L_{1v}), −5.25 (L_{1v}), −0.94 (L_{3v}), 1.96 (L_{1c}), and 4.87 (L_{3c}) eV. Our results generally agree with theirs, although definite differences exist in Γ_{15c} and L_{1v}, probably caused by the present calculation having insufficient plane-wave bases for Zn compounds, and by the treatment of 3*d* electrons as core states. Regarding WZ's electronic structures, Salehpour and Satpathy[25] calculated the band structures of diamond by the linear-muffin-tin-orbital (LMTO) method under the LDA, and when their combined correction to the atomic-sphere approximation (ASA) is included, they obtained the valence-band width and the band-gap energies of 21.2, 5.7 (Γ_{15c}), and 4.7 (X_{1c}) eV for ZB, and 21.4, 4.2 (Γ_{6c}), and 3.0 (K_{2c}) eV for WZ. These values compare well with our corresponding results of 21.6, 5.6 (Γ_{15c}), and 4.5 (X_{1c}) eV for ZB, and 21.9, 4.7 (Γ_{6c}), and 3.0 (K_{2c}) eV for WZ.

Next we discuss where the lowest conduction-band state is located in the Brillouin zone, and compare the band structures of ZB and WZ. As shown in Table III, all the II-VI and III-V semiconductors in the ZB structures, except the Al compounds and GaP, have Γ_{1c}^{ZB} as the lowest conduction-band state, i.e., direct-band-gap materials, whereas the others are indirect-gap semiconductors with the lowest conduction-band state X_{1c}^{ZB}. In the WZ structure (Table IV), however, all semiconductors which have direct band gaps in ZB also have the lowest conduction-band state Γ_{1c}^{WZ} (or Γ_{3c}^{WZ} for GaSb) and are direct-band-gap materials.

The indirect-gap semiconductors in ZB show several different characteristies in their lowest conduction-band states when their crystal structures are changed into WZ. As mentioned in Sec. II, because WZ states at U^{WZ} have the same wave numbers as ZB states at LX^{ZB}, and because the lowest conduction band of ZB often shows extremes at LX^{ZB}, the lowest conduction-band state at U^{WZ} or that at the points L^{WZ} and M^{WZ} near U^{WZ} are expected to have the lowest energy in the whole Brillouin zone, which is the case for Si, AlP, and AlAs (M_{1c}^{WZ}). On the other hand, the energies of the lowest conduction-band states at these points were found to increase compared with those at Γ^{WZ}. Consequently, AlN, AlSb, and GaP become semiconductors with a direct band gap. Especially in AlSb and GaP, the lowest conduction-band states are Γ_{3c}^{WZ}, which have characteristics similar to the L_{1c}^{ZB} states of ZB. This occurs because the states at one of the four L^{ZB} points of ZB are folded into the states at Γ^{WZ} of WZ, and also because the L_{1c}^{ZB} state has a lower energy value than that of Γ_{1c}^{ZB} in ZB. In C and SiC we obtained the lowest conduction-band state at K_{2c}^{WZ}, which has no apparent correspondence to a state in ZB.

TABLE III. Energies (eV) of representative states at symmetry points, relative to the valence-band maximum, for various semiconductors with a ZB structure, and the four lowest conduction-band states in ascending order. The numbers in parentheses indicate degeneracy of the states.

Material	Γ_{1v}	Γ_{1c}	$\Gamma_{15c}(3)$	L_{1v}	L_{1v}	$L_{3v}(2)$	L_{1c}	$L_{3c}(2)$	X_{1v}	X_{3v}	$X_{5v}(2)$	X_{1c}	X_{3c}	Order
C	−21.581	13.336	5.570	−15.715	−13.507	−2.781	8.794	8.360	−12.797	−12.797	−6.326	4.502	4.502	$X_{1c}X_{3c}\Gamma_{15c}L_{3c}$
Si	−11.962	3.314	2.558	−9.610	−6.981	−1.190	1.513	3.332	−7.805	−7.805	−2.850	0.634	0.634	$X_{1c}X_{3c}L_{1c}\Gamma_{15c}$
SiC	−15.598	5.961	7.067	−12.032	−8.668	−1.039	5.136	6.985	−10.585	−7.917	−3.221	1.108	4.017	$X_{1c}X_{3c}L_{1c}\Gamma_{1c}$
AlN	−15.675	3.366	11.816	−13.797	−6.034	−0.434	6.597	10.497	−13.222	−5.110	−1.807	2.882	7.905	$X_{1c}\Gamma_{1c}L_{1c}X_{3c}$
AlP	−11.353	3.367	4.613	−9.653	−5.509	−0.745	2.846	4.845	−8.935	−5.290	−2.071	1.560	2.433	$X_{1c}X_{3c}L_{1c}\Gamma_{1c}$
AlAs	−11.857	2.003	4.289	−10.426	−5.562	−0.805	2.092	4.654	−9.882	−5.417	−2.147	1.363	2.212	$X_{1c}\Gamma_{1c}L_{1c}X_{3c}$
AlSb	−10.667	1.628	3.148	−9.270	−5.405	−0.887	1.338	3.736	−8.665	−5.482	−2.164	1.170	1.378	$X_{1c}L_{1c}X_{3c}\Gamma_{1c}$
GaN	−16.661	1.467	10.110	−14.532	−7.243	−0.880	4.410	10.143	−13.860	−6.426	−2.673	2.938	6.482	$\Gamma_{1c}X_{1c}L_{1c}X_{3c}$
GaP	−12.226	2.101	4.046	−10.253	−6.508	−1.055	1.862	4.836	−9.364	−6.641	−2.583	1.679	1.853	$X_{1c}X_{3c}L_{1c}\Gamma_{1c}$
GaAs	−12.596	0.614	3.799	−10.969	−6.543	−1.090	1.043	4.661	−10.270	−6.717	−2.595	1.421	1.636	$\Gamma_{1c}L_{1c}X_{1c}X_{3c}$
GaSb	−11.394	0.247	2.852	−9.806	−6.319	−1.121	0.490	3.789	−8.988	−6.747	−2.530	0.890	1.216	$\Gamma_{1c}L_{1c}X_{1c}X_{3c}$
InP	−11.102	1.116	4.320	−9.627	−5.489	−0.855	1.737	4.942	−8.954	−5.536	−2.115	1.817	2.333	$\Gamma_{1c}L_{1c}X_{1c}X_{3c}$
InAs	−11.535	0.074	4.035	−10.342	−5.543	−0.886	1.109	4.718	−9.858	−5.638	−2.137	1.548	2.076	$\Gamma_{1c}L_{1c}X_{1c}X_{3c}$
InSb	−10.454	0.043	3.086	−9.225	−5.437	−0.920	0.672	3.867	−8.664	−5.730	−2.117	1.350	1.356	$\Gamma_{1c}L_{1c}X_{1c}X_{3c}$
ZnS	−11.597	3.563	7.307	−10.497	−4.295	−0.555	4.453	7.557	−10.198	−4.032	−1.556	3.838	4.691	$\Gamma_{1c}X_{1c}L_{1c}X_{3c}$
ZnSe	−12.237	2.314	6.310	−11.370	−4.433	−0.610	3.307	6.652	−11.130	−4.243	−1.661	3.198	3.809	$\Gamma_{1c}X_{1c}L_{1c}X_{3c}$
ZnTe	−11.085	1.952	4.783	−10.180	−4.548	−0.690	2.288	5.255	−9.845	−4.483	−1.767	2.508	2.525	$\Gamma_{1c}L_{1c}X_{1c}X_{3c}$
CdS	−10.982	2.472	7.343	−10.360	−3.549	−0.454	3.996	7.518	−10.044	−3.350	−1.253	3.903	4.915	$\Gamma_{1c}X_{1c}L_{1c}X_{3c}$
CdSe	−11.745	1.577	6.448	−11.184	−3.721	−0.502	3.141	6.716	−10.950	−3.573	−1.340	3.348	4.137	$\Gamma_{1c}L_{1c}X_{1c}X_{3c}$
CdTe	−10.457	1.475	4.993	−9.806	−3.824	−0.558	2.351	5.393	−9.579	−3.793	−1.444	2.749	2.930	$\Gamma_{1c}L_{1c}X_{1c}X_{3c}$
HgS	−11.332	1.539	7.325	−10.357	−4.133	−0.537	3.254	7.707	−10.030	−4.121	−1.408	4.148	4.214	$\Gamma_{1c}L_{1c}X_{1c}X_{3c}$
HgSe	−11.948	0.607	6.392	−11.282	−4.335	−0.581	2.344	6.827	−11.031	−4.376	−1.486	3.475	3.497	$\Gamma_{1c}L_{1c}X_{1c}X_{3c}$
HgTe	−10.872	0.473	4.960	−10.077	−4.540	−0.649	1.627	5.493	−9.775	−4.706	−1.614	2.403	2.832	$\Gamma_{1c}L_{1c}X_{1c}X_{3c}$

TABLE IV. Energies (eV) of representative states at symmetry points, relative to the valence-band maximum, for various semiconductors with a WZ structure, and the four lowest conduction-band states in ascending order. The numbers in parentheses indicate degeneracy of the states.

Material	Γ_{1c}	Γ_{3c}	$\Gamma_{6c}(2)$	$A_{56v}(4)$	$A_{13c}(2)$	$L_{13v}(2)$	$L_{13c}(2)$	U_{4v}	U_{3c}	M_{4v}	M_{1c}	$H_{3v}(2)$	$H_{3c}(2)$	K_{2v}	K_{2c}	Order
C	14.073	7.580	4.686	−1.974	7.332	−4.709	5.484	−4.255	4.661	−3.043	3.980	−4.182	7.618	−6.942	3.020	$K_{2c}M_{1c}U_{3c}\Gamma_{6c}$
Si	3.457	0.883	1.941	−0.966	1.685	−2.396	0.875	−2.008	0.662	−1.416	0.290	−1.930	1.615	−3.298	0.755	$M_{1c}U_{3c}K_{2c}L_{13c}$
SiC	5.984	4.426	6.372	−0.727	5.553	−2.374	3.019	−1.907	2.766	−1.170	2.452	−1.753	4.846	−3.875	2.001	$K_{2c}M_{1c}U_{3c}L_{13c}$
AlN	3.472	6.218	10.826	−0.267	6.079	−1.263	4.853	−0.905	4.456	−0.479	5.428	−0.793	7.191	−2.372	4.602	$\Gamma_{1c}U_{3c}K_{2c}L_{13c}$
AlP	3.400	2.414	4.275	−0.508	3.292	−1.610	2.337	−1.261	2.136	−0.823	1.907	−1.186	3.171	−2.407	2.197	$M_{1c}U_{3c}K_{2c}L_{13c}$
AlAs	2.045	1.703	3.955	−0.542	2.504	−1.682	1.899	−1.328	1.696	−0.887	1.646	−1.265	2.711	−2.445	2.098	$M_{1c}U_{3c}\Gamma_{3c}L_{13c}$
AlSb	1.655	0.972	2.848	−0.605	1.686	−1.735	1.306	−1.399	1.179	−0.971	1.073	−1.359	1.953	−2.398	1.667	$\Gamma_{3c}M_{1c}U_{3c}L_{13c}$
GaN	1.588	4.032	9.666	−0.480	4.222	−1.917	4.072	−1.453	3.749	−0.911	4.718	−1.479	6.108	−2.891	4.776	$\Gamma_{1c}U_{3c}\Gamma_{3c}L_{13c}$
GaP	2.147	1.432	3.758	−0.692	2.282	−2.038	1.809	−1.636	1.679	−1.135	1.529	−1.611	2.655	−2.777	2.262	$\Gamma_{3c}M_{1c}U_{3c}L_{13c}$
GaAs	0.647	0.670	3.500	−0.713	1.461	−2.058	1.319	−1.662	1.132	−1.170	1.254	−1.645	2.146	−2.765	2.185	$\Gamma_{1c}\Gamma_{3c}U_{3c}M_{1c}$
GaSb	0.260	0.134	2.554	−0.757	0.842	−2.049	0.775	−1.679	0.630	−1.209	0.742	−1.669	1.484	−2.688	1.695	$\Gamma_{3c}\Gamma_{1c}U_{3c}M_{1c}$
InP	1.200	1.445	4.132	−0.528	2.098	−1.630	1.939	−1.299	1.760	−0.900	1.897	−1.297	2.742	−2.209	2.602	$\Gamma_{1c}\Gamma_{3c}U_{3c}M_{1c}$
InAs	0.114	0.810	3.824	−0.551	1.444	−1.660	1.499	−1.331	1.288	−0.931	1.606	−1.333	2.267	−2.223	2.477	$\Gamma_{1c}\Gamma_{3c}U_{3c}A_{13c}$
InSb	0.072	0.385	2.869	−0.592	1.002	−1.681	1.050	−1.366	0.890	−0.976	1.099	−1.370	1.685	−2.201	2.006	$\Gamma_{1c}\Gamma_{3c}U_{3c}A_{13c}$
ZnS	3.588	4.132	7.100	−0.336	4.782	−1.153	4.351	−0.889	4.148	−0.587	4.243	−0.855	5.321	−1.780	4.716	$\Gamma_{1c}\Gamma_{3c}U_{3c}M_{1c}$
ZnSe	2.324	3.031	6.113	−0.371	3.609	−1.232	3.444	−0.958	3.246	−0.642	3.416	−0.924	4.313	−1.864	4.072	$\Gamma_{1c}\Gamma_{3c}U_{3c}M_{1c}$
ZnTe	1.985	2.011	4.591	−0.428	2.677	−1.355	2.449	−1.070	2.312	−0.731	2.341	−1.051	3.150	−1.965	3.105	$\Gamma_{1c}\Gamma_{3c}U_{3c}M_{1c}$
CdS	2.526	3.792	7.180	−0.263	4.019	−0.915	4.172	−0.706	3.974	−0.473	4.420	−0.700	5.111	−1.367	4.916	$\Gamma_{1c}\Gamma_{3c}U_{3c}A_{13c}$
CdSe	1.623	2.934	6.277	−0.302	3.205	−1.004	3.437	−0.782	3.231	−0.531	3.675	−0.770	4.276	−1.470	4.323	$\Gamma_{1c}\Gamma_{3c}A_{13c}U_{3c}$
CdTe	1.501	2.133	4.851	−0.330	2.621	−1.084	2.645	−0.851	2.492	−0.580	2.699	−0.842	3.301	−1.545	3.461	$\Gamma_{1c}\Gamma_{3c}U_{3c}A_{13c}$
HgS	1.618	3.045	7.217	−0.304	3.224	−1.033	3.707	−0.806	3.533	−0.553	3.978	−0.825	4.499	−1.442	5.146	$\Gamma_{1c}\Gamma_{3c}A_{13c}U_{3c}$
HgSe	0.641	2.112	6.263	−0.334	2.445	−1.108	2.920	−0.868	2.723	−0.601	3.248	−0.886	3.691	−1.533	4.511	$\Gamma_{1c}\Gamma_{3c}A_{13c}U_{3c}$
HgTe	0.496	1.411	4.833	−0.377	1.905	−1.217	2.132	−0.965	1.989	−0.671	2.319	−0.973	2.810	−1.663	3.553	$\Gamma_{1c}\Gamma_{3c}A_{13c}U_{3c}$

Taken together, our results for indirect-gap semiconductors with a ZB structure suggest that we can roughly estimate the WZ band structure around the fundamental gap via the knowledge acquired about the ZB band structure. When the energy difference between X_{1c}^{ZB} and the lower state of Γ_{1c}^{ZB} or L_{1c}^{ZB} in the ZB structure is less than about 0.5 eV, indirect-gap materials with a ZB structure may possibly have a direct band gap in the WZ structure, whereas for other indirect-gap semiconductors in the ZB structure they survive as indirect ones in WZ with the lowest conduction-band state at M^{WZ} or K^{WZ}.

IV. BAND OFFSETS

The band offset is an essential quantity for obtaining characterization information about a system's electronic structure. Most band-edge states around the fundamental gap appear on the ΓL^{ZB}-Z^{ZB} and V^{ZB}-LX^{ZB} lines in ZB, and on Γ^{WZ}-A^{WZ} and M^{WZ}-L^{WZ} lines in WZ (Sec. III), because these lines have high crystal symmetry. In addition, a considerable difference exists in the magnitude of offset between "zone-center" and "zone-boundary" states. We designate the states around the ΓL^{ZB}-Z^{ZB} line in ZB, or the Γ^{WZ}-A^{WZ} line in WZ as zone-center states; while those away from these lines, such as the states around V^{ZB}-LX^{ZB} in ZB or M^{WZ}-L^{WZ} in WZ, are called zone-boundary ones. The zone-center states have small wave numbers perpendicular to [111], while the zone-boundary states have large wave numbers perpendicular to [111]. Birman,[24] using the tight-binding method, was the first to point out that the zone-center states of WZ can be obtained by perturbing corresponding states of ZB, though no apparent correspondence occurs between zone-boundary states of WZ and ZB. Therefore, we will subsequently concentrate attention on band offsets for the states on these lines, and individually present the results for zone-center and zone-boundary states.

A. Zone-center state

Table V shows the calculated results of band offsets for various semiconductors, where representative states at ΓL^{ZB} in ZB and Γ^{WZ} point in WZ are considered. All band offsets are calculated by subtracting the energy of the state in ZB from that of the corresponding state in WZ, such as $E^{WZ}-E^{ZB}$ (Sec. II). Since WZ has lower symmetry than ZB, some degenerate states in ZB split into two groups in WZ, and in such cases we present only the offset of one state and the splitting energy.

Although the order and values of energy levels are different among various states and semiconductors (Table V), each particular offset and splitting energy has a definite sign independent of the material. Therefore, this allows us to characterize generally the change in energy level going from ZB to WZ structures. Figure 3 schematically shows the band offset between states at ΓL^{ZB} in ZB, and the corresponding states at Γ^{WZ} in WZ. Because

TABLE V. Calculated band offsets between the states at the ΓL^{ZB} point in ZB and those at the Γ^{WZ} point in WZ, and the splitting energies of states which are degenerated in the ZB structure. The Γ_{15v}^{ZB} and Γ_{15c}^{ZB} states in ZB, respectively, split into $\Gamma_{6v}^{WZ}+\Gamma_{1v}^{WZ}$ and $\Gamma_{6c}^{WZ}+\Gamma_{1c}^{WZ}$ in WZ.

	Band offset (eV)					Splitting energy (eV)	
Material	$\Gamma_{5v}^{WZ}-L_{3v}^{ZB}$	$\Gamma_{6v}^{WZ}-\Gamma_{15v}^{ZB}$	$\Gamma_{1c}^{WZ}-\Gamma_{1c}^{ZB}$	$\Gamma_{3c}^{WZ}-L_{1c}^{ZB}$	$\Gamma_{6c}^{WZ}-\Gamma_{15c}^{ZB}$	$\Gamma_{6v}^{WZ}-\Gamma_{1v}^{WZ}$	$\Gamma_{1c}^{WZ}-\Gamma_{6c}^{WZ}$
C	−0.203	0.286	1.023	−0.928	−0.597	0.488	1.094
Si	−0.151	0.234	0.378	−0.395	−0.382	0.287	0.603
SiC	−0.164	0.145	0.169	−0.565	−0.548	0.153	1.126
AlN	−0.085	0.056	0.162	−0.322	−0.932	0.092	1.329
AlP	−0.101	0.081	0.114	−0.350	−0.256	0.088	0.579
AlAs	−0.091	0.085	0.127	−0.302	−0.248	0.089	0.531
AlSb	−0.082	0.085	0.112	−0.281	−0.215	0.109	0.478
GaN	−0.078	0.034	0.154	−0.344	−0.409	0.140	0.800
GaP	−0.091	0.081	0.126	−0.348	−0.206	0.121	0.519
GaAs	−0.079	0.084	0.117	−0.289	−0.214	0.122	0.501
GaSb	−0.077	0.089	0.102	−0.266	−0.209	0.149	0.480
InP	−0.059	0.045	0.129	−0.245	−0.142	0.082	0.401
InAs	−0.062	0.046	0.086	−0.252	−0.164	0.099	0.408
InSb	−0.058	0.057	0.086	−0.230	−0.160	0.108	0.390
ZnS	−0.050	0.033	0.057	−0.287	−0.173	0.038	0.437
ZnSe	−0.056	0.026	0.036	−0.249	−0.170	0.049	0.417
ZnTe	−0.056	0.039	0.072	−0.237	−0.151	0.057	0.038
CdS	−0.031	0.019	0.073	−0.184	−0.143	0.031	0.358
CdSe	−0.026	0.030	0.076	−0.176	−0.140	0.029	0.357
CdTe	−0.044	0.021	0.048	−0.196	−0.119	0.029	0.321
HgS	−0.028	0.015	0.093	−0.194	−0.092	0.036	0.329
HgSe	−0.037	0.017	0.052	−0.213	−0.111	0.046	0.328
HgTe	−0.035	0.022	0.045	−0.193	−0.104	0.039	0.312

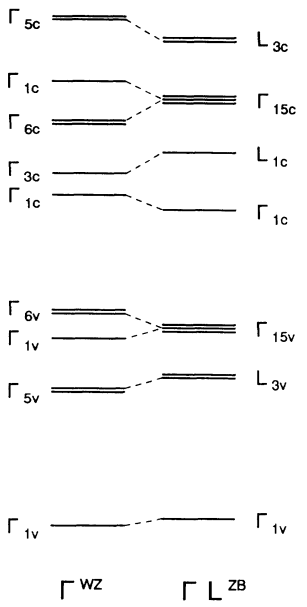

FIG. 3. Schematic diagram of band offsets between the states at the ΓL^{ZB} point in ZB and those at Γ^{WZ} in WZ, where the dashed lines indicate correspondence between states.

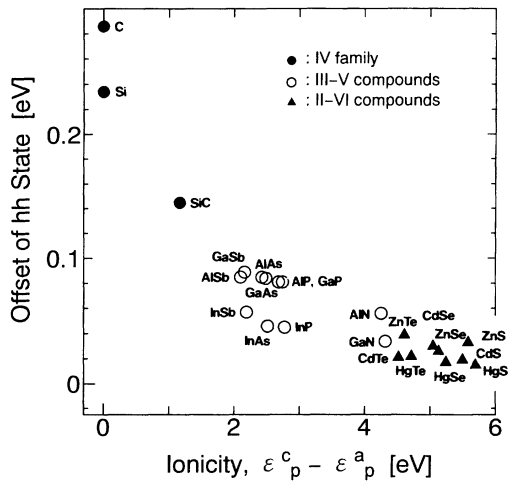

FIG. 4. Calculated band offsets for the heavy-hole states of various semiconductors as a function of ionicity.

the top of the valence band (heavy-hole states) always doubly degenerates in WZ, a hole in the WZ/ZB system will be localized in the WZ layers. Chou, Cohen, and Louie[23] calculated the electronic structure of stacking faults in Si and found the defect state, localized around the stacking faults (WZ layers) and having an energy 0.1 eV above the valence-band maximum of ZB, to be consistent with a photoluminescence experiment.[53] Mattheiss and Patel[28] also calculated electronic stacking-fault states in Si using the nonorthogonal-tight-binding method, and found similar states located about 0.1 eV above the valence-band maximum. Our result showing a heavy-hole offset in Si is in good agreement with these calculations. On the other hand, with respect to the conduction-band states of direct-gap semiconductors, since the lowest electron state is localized in ZB layers this suggests that a WZ/ZB system made of a direct-gap semiconductor is a type-II superlattice, where the electron and hole are localized in different layers. The only exception is for GaSb, in which case the system is a type-I superlattice because Γ_{3c}^{WZ} is the lowest conduction-band state.

The next question we considered was how the band offset changes with respect to different materials. Figure 4 shows the calculated band offsets of the heavy-hole states (Γ_{15v}^{ZB} vs Γ_{6v}^{WZ}) as a function of ionicity, which is defined as the difference between the p-orbital energies of cation and anion free atoms. These atomic p-orbital energies are calculated under the LDA for a free atom with a ground-state neutral electron configuration, the method being the same as that of Bachelet, Hamann, and Schlüter.[37] As seen in Fig. 4, there appears to be a clear chemical trend that the offset decreases in a monotonous manner with increasing ionicity. Of particular interest is that this chemical trend applies to other states in Table V. Moreover, when we compared states with the same symmetry (e.g., Γ_{15v}^{ZB} and Γ_{15c}^{ZB}), it was discovered that the offsets are larger for the conduction-band states than for the valence-band ones.

To analyze these results, we employed the standard sp^3-tight-binding method.[54] Corresponding notations and analyses of Hamiltonian matrices are explained in the Appendix, and therefore only the results are given here. The resultant energies of the Γ_{15v}^{ZB} and Γ_{15c}^{ZB} states in ZB, and those of Γ_{6v}^{WZ} and Γ_{6c}^{WZ} in WZ, respectively, are given as

$$E(\Gamma_{15v}^{ZB},\Gamma_{15c}^{ZB})=\frac{\tilde{\varepsilon}_p^c+\tilde{\varepsilon}_p^a}{2}\mp\left[\left[\frac{\tilde{\varepsilon}_p^c-\tilde{\varepsilon}_p^a}{2}\right]^2+(\tfrac{4}{3}U_{pp\sigma}^{ca}+\tfrac{8}{3}U_{pp\pi}^{ca})^2\right]^{1/2}, \tag{3}$$

$$E(\Gamma_{6v}^{WZ},\Gamma_{6c}^{WZ})=\frac{\tilde{\varepsilon}_p^c+\tilde{\varepsilon}_p^a}{2}\mp\left[\left[\frac{\tilde{\varepsilon}_p^c-\tilde{\varepsilon}_p^a}{2}\right]^2+(\tfrac{4}{3}U_{pp\sigma}^{ca}+\tfrac{8}{3}U_{pp\pi}^{ca}+W_{pp\pi}^{ca})^2\right]^{1/2}, \tag{4}$$

where the Γ_{15v}^{ZB} and Γ_{6v}^{WZ} (Γ_{15c}^{ZB} and Γ_{6c}^{WZ}) states have a negative (positive) sign, U, V, and W, respectively, are the transfer energies between the first, second, and third-nearest-neighboring sites, and

$$\tilde{\varepsilon}_p^c=\varepsilon_p^c+4V_{pp\sigma}^{cc}+8V_{pp\pi}^{cc}, \tag{5}$$

$$\tilde{\varepsilon}_p^a=\varepsilon_p^a+4V_{pp\sigma}^{aa}+8V_{pp\pi}^{aa}, \tag{6}$$

with ε_p^c and ε_p^a indicating the on-site energies of the p or-

bitals of cation and anion atoms. The band offset of the heavy-hole state is defined as $\Delta E_{\rm hh}=E(\Gamma_{6v}^{\rm WZ})-E(\Gamma_{15v}^{\rm ZB})$. Because W is relatively small compared with U and V, we obtain the band-offset energy as

$$\Delta E_{hh}\simeq-\frac{(4/3U_{pp\sigma}^{\rm ca}+8/3U_{pp\pi}^{\rm ca})W_{pp\pi}^{\rm ca}}{\sqrt{\{(\bar{\varepsilon}_p^c-\bar{\varepsilon}_p^a)/2\}^2+(4/3U_{pp\sigma}^{\rm ca}+8/3U_{pp\pi}^{\rm ca})^2}}\ . \tag{7}$$

By comparing the results from the first-principles calculation and Eq. (7), we reached three conclusions: (1) The band offset of the heavy-hole state appears due to the existence of W. In order to explain this in more detail, the number of nearest-neighboring sites for a particular origin site is summarized in Table VI for the WZ and ZB crystal structures. Note that the real length (a.u.) between the corresponding neighboring sites is given in the distance column for the case of Si. As indicated, WZ and ZB have the same surroundings for the second-nearest-neighboring site; thus there is no difference in transfer energy between $E(\Gamma_{15v}^{\rm ZB})$ and $E(\Gamma_{6v}^{\rm WZ})$. Only at the third-nearest-neighboring site does a difference appear. In our tight-binding analysis, we considered only the transfer energy in WZ having the shortest neighboring length (7.393 a.u.) among the four possibilities, since this transfer energy has nearly the same neighboring length as that of the corresponding second-nearest-neighboring site (7.244 a.u.). It is therefore this difference between the third-nearest-neighboring sites in WZ and ZB that causes the band offset. (2) The band offset at the WZ/ZB interface has a definite sign. Because $(4/3U_{pp\sigma}^{\rm ca}+8/3U_{pp\pi}^{\rm ca})>0$ and $W_{pp\pi}^{\rm ca}<0$, ΔE_{hh} has a positive value, being consistent with the first-principles calculation. (3) The magnitude of the band offset is determined by the competition between ionicity and covalency, as can be seen in the denominator of Eq. (7), where $(\bar{\varepsilon}_p^c-\bar{\varepsilon}_p^a)/2$ corresponds to ionicity and $(4/3U_{pp\sigma}^{\rm ca}+8/3U_{pp\pi}^{\rm ca})$ to covalency. Obviously, the offset becomes large when the ionicity $\bar{\varepsilon}_p^c-\bar{\varepsilon}_p^a$ is small, a phenomena that reflects the fact that the band offset is affected by chemical composition, as determined by the first-principles calculation.

TABLE VI. Number of nth-nearest neighboring sites from a particular (origin) site in both WZ and ZB structures, distances from the origin site to nth-nearest-neighboring sites, and symbols of the corresponding transfer energies. The nth-nearest-neighboring site is defined such that it takes at least n bonds to go from the origin site to the nth-nearest-neighboring site. Four kinds of third-nearest-neighboring sites exist in WZ, which have different distances, while only two exist in ZB. Distances are shown in the case of Si.

Neighbor	WZ	ZB	Distance (a.u.)	Transfer energy
First	4	4	4.436	$U^{\rm ca}, U^{\rm ac}$
Second	12	12	7.244	$V^{\rm cc}, V^{\rm aa}$
Third	1		7.393	$W^{\rm ca}, W^{\rm ac}$
	9	12	8.494	
	6		10.351	
	9	12	11.164	
Fourth	6	6	10.245	

Even though we only investigated the offset for the heavy-hole states, the same type of analysis applies to the pairs of other states, e.g., $(\Gamma_{6c}^{\rm WZ},\Gamma_{15c}^{\rm ZB})$, $(\Gamma_{5v}^{\rm WZ},L_{3v}^{\rm ZB})$, and $(\Gamma_{5c}^{\rm WZ},L_{3c}^{\rm ZB})$. (The equations of the energies for the latter two pairs are presented in the Appendix.) As for pairs in other states such as $(\Gamma_{1c}^{\rm WZ},\Gamma_{1c}^{\rm ZB})$ and $(\Gamma_{3c}^{\rm WZ},L_{1c}^{\rm ZB})$, although a simple analytic formula cannot be derived via the sp^3-tight-binding method, the same band-offset mechanism is applicable because these states also show similar characteristic features in their offset. On the other hand, it is difficult to use this method to explain why band offsets are larger for conduction-band states than for the valence-band ones. We calculated the offset between $\Gamma_{6c}^{\rm WZ}$ and $\Gamma_{15c}^{\rm ZB}$ to be as large as that between $\Gamma_{6v}^{\rm WZ}$ and $\Gamma_{15v}^{\rm ZB}$, but with a different sign: a result in disagreement with first-principles results. One possible reason for this discrepancy is that sp^3-tight-binding method is not suitable for analyzing the conduction-band states[55] due to the limited number of expansion bases.

B. Zone-boundary state

Since the $LX^{\rm ZB}$ point corresponds to the $U^{\rm WZ}$ point in the sense that both points have the same wave numbers in **k** space (Sec. II), here we consider the band offsets occurring between these points. Figure 5 is a diagram of the energy spectra at these points, where a correspondence between the energy and symmetry of states for WZ and ZB exists only for some states; hence we examine these states first. Table VII summarizes band offsets for various semiconductors. The band offset between states $L_{3v}^{\rm ZB}$ and $U_{4v}^{\rm WZ}$ is shown in Fig. 6 as a function of ionicity.

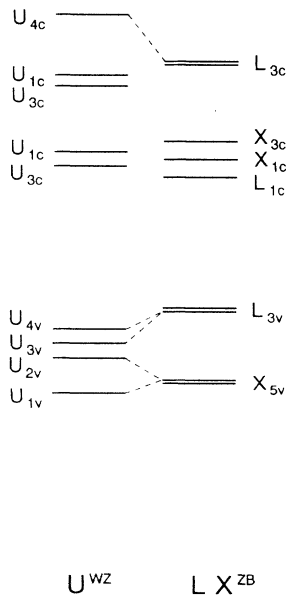

FIG. 5. Schematic diagram of band offsets between the states at the $LX^{\rm ZB}$ point in ZB and those at $U^{\rm WZ}$ in WZ, where the dashed lines indicate correspondence between states.

TABLE VII. Calculated band offsets between the states at the LX^{ZB} point in ZB and those at the U^{WZ} point in WZ, and the splitting energies of states which are degenerated in the ZB structure. The X_{5v}^{ZB} and L_{3v}^{ZB} states in ZB, respectively, split into $U_{2v}^{WZ}+U_{1v}^{WZ}$ and $U_{4v}^{WZ}+U_{3v}^{WZ}$ in WZ.

Material	Band offset (eV) $U_{2v}^{WZ}-X_{5v}^{ZB}$	Band offset (eV) $U_{4v}^{WZ}-L_{3v}^{ZB}$	Band offset (eV) $U_{4c}^{WZ}-L_{3c}^{ZB}$	Splitting energy (eV) $U_{2v}^{WZ}-U_{1v}^{WZ}$	Splitting energy (eV) $U_{4v}^{WZ}-U_{3v}^{WZ}$
C	0.655	−1.188	2.274	0.227	0.203
Si	0.286	−0.583	1.282	0.574	0.086
SiC	0.401	−0.723	1.672	0.592	0.169
AlN	0.277	−0.413	1.213	0.607	0.173
AlP	0.241	−0.434	1.117	0.473	0.089
AlAs	0.249	−0.437	1.092	0.513	0.088
AlSb	0.231	−0.426	0.988	0.483	0.076
GaN	0.370	−0.539	1.115	0.604	0.156
GaP	0.285	−0.500	1.162	0.545	0.084
GaAs	0.284	−0.487	1.142	0.593	0.084
GaSb	0.260	−0.468	1.046	0.565	0.077
InP	0.244	−0.397	0.939	0.464	0.072
InAs	0.242	−0.398	0.942	0.501	0.073
InSb	0.226	−0.388	0.900	0.478	0.065
ZnS	0.201	−0.301	0.970	0.351	0.075
ZnSe	0.211	−0.321	0.969	0.388	0.078
ZnTe	0.207	−0.340	0.937	0.403	0.076
CdS	0.167	−0.232	0.750	0.286	0.061
CdSe	0.167	−0.249	0.784	0.316	0.062
CdTe	0.177	−0.271	0.781	0.324	0.061
HgS	0.183	−0.253	0.716	0.325	0.058
HgSe	0.183	−0.270	0.766	0.363	0.062
HgTe	0.195	−0.293	0.799	0.383	0.061

Based on Table VII and Fig. 6, as well as the results from the zone-center states, we found that the offset has a definite sign, shows a clear chemical trend, and is larger for the conduction-band states than for the valence-band ones; these are phenomena which can all be explained similarly to the case of zone-center states. In addition, when the offset values in Tables V and VII are compared, the band offset as a whole is noticeably much larger for the zone-boundary than for the zone-center states. For example, in the case of the L_{3v}^{ZB} states in ZB for C, which have distinct corresponding states Γ_{5v}^{WZ} and U_{4v}^{WZ} in WZ, the band offset is −1.19 eV for the zone-boundary state ($U_{4v}^{WZ}-L_{3v}^{ZB}$), while it is −0.20 eV for the zone-center state ($\Gamma_{5v}^{WZ}-L_{3v}^{ZB}$).

Let us again analyze the above band offset results by the sp^3-tight-binding method, considering as an example the L_{3v}^{ZB} and U_{4v}^{WZ} states whose energy levels are respectively given as

$$E(L_{3v}^{ZB},L_{3c}^{ZB})=\frac{\varepsilon_p^c+\varepsilon_p^a}{2}\mp\left[\left[\frac{\varepsilon_p^c-\varepsilon_p^a}{2}\right]^2+(\tfrac{4}{3}U_{pp\sigma}^{ca}+\tfrac{2}{3}U_{pp\pi}^{ca})^2\right]^{1/2}, \tag{8}$$

$$E(U_{4v}^{WZ},U_{4c}^{WZ})=\frac{\varepsilon_p^c+\varepsilon_p^a}{2}\mp\left[\left[\frac{\varepsilon_p^c-\varepsilon_p^a}{2}\right]^2+|\tfrac{4}{3}e^{i2\pi/3}U_{pp\sigma}^{ca}+(-1-\tfrac{1}{3}e^{i2\pi/3})U_{pp\pi}^{ca}|^2\right]^{1/2}, \tag{9}$$

where only the on-site and first-nearest-neighboring transfer energies are taken into account. It should be noted that the difference in energy between L_{3v}^{ZB} and U_{4v}^{WZ} is presented in the first-nearest-neighboring transfer energy, which is in marked contrast to the zone-center states. The origin of this difference can be traced by evaluating their Hamiltonian matrices shown in the Appendix. As indicated, the Hamiltonian matrix of WZ and ZB has a different phase in the off-diagonal (transfer) part, being caused by a difference in their respective atomic positions. From the standpoint of a superlattice, this difference in phase can be expressed as the difference in the continuity condition of a wave function, i.e., phase matching. Consequently, because the transfer energy of the first-nearest-neighboring site is larger than that of the third, the offset energy is large at the boundary of Brillouin zone, while it is small at the center.

On the other hand, it is difficult to establish a clear correspondence between WZ and ZB states in the conduction bands, except for the L_{3c}^{ZB} and U_{4c}^{WZ} states, which are shown in Fig. 5. A probable explanation for this is that when the WZ/ZB interface is produced, and the translational symmetry along the [111] direction is broken, states which have the same wave numbers perpen-

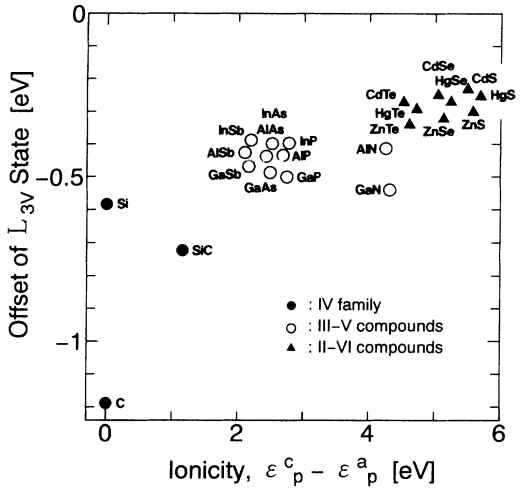

FIG. 6. Calculated band offsets between the L_{3v}^{ZB} states in ZB and the U_{4v}^{WZ} states in WZ as a function of ionicity.

dicular to [111] and different wave vectors parallel to [111] generally hybridize each other. As mentioned in Sec. II, when the same Brillouin zone is considered for both structures, a correspondence is possible between groups of points. This is especially true in the present case; because the lower conduction-band states at LX^{ZB}, V_1^{ZB}, and V_2^{ZB} have similar energies and the same symmetry in WZ, and since they strongly hybridize to make new, lower conduction-band states at M^{WZ}, U_1^{WZ}, and U_2^{WZ}. Thus it is difficult to show correspondence between the conduction-band states of LX^{ZB} and those of U^{WZ}.

Nevertheless, it is still practically useful, especially for indirect-gap semiconductor materials, to examine where their lowest conduction-band states appear on the V^{ZB}-LX^{ZB} line in ZB, and the M^{WZ}-L^{WZ} line in WZ. Table VIII lists the representations of these states and the energy differences between them. For most indirect-gap materials that have their lowest conduction-band state at X^{ZB} in ZB, this state appears at M^{WZ} in WZ. In addition, in C, Si, AlSb, and GaP, the lowest conduction-band state in WZ (M_{1c}^{WZ}) has a lower energy than that in ZB (X_{1c}^{ZB} or X_{13c}^{ZB}), whereas in other indirect-gap materials the energy of the former state (M_{1c}^{WZ}) is higher. The result for Si is consistent with calculations by Chou, Cohen, and Louie,[23] who found the lowest conduction-band state to be localized in WZ layers. Taking the results of the zone-center and zone-boundary states together, we conclude that the WZ/ZB homomaterial systems of C, Si, AlSb, and GaP are of type I, while those of other semiconductors are type II.

TABLE VIII. Energy difference between the lowest conduction-band state at either the M^{WZ} or U^{WZ} point in WZ and at either the X^{ZB} or L^{ZB} point in ZB, for various semiconductors. The WZ and ZB columns indicate representations of these states, and the number in parentheses denotes the degeneracy.

Material	Difference (eV)	WZ	ZB
C	−0.236	M_{1c}	$X_{13c}(2)$
Si	−0.109	M_{1c}	$X_{13c}(2)$
SiC	1.489	M_{1c}	X_{1c}
AlN	1.630	U_{3c}	X_{1c}
AlP	0.429	M_{1c}	X_{1c}
AlAs	0.369	M_{1c}	X_{1c}
AlSb	−0.012	M_{1c}	X_{1c}
GaN	0.844	U_{3c}	X_{1c}
GaP	−0.068	M_{1c}	X_{1c}
GaAs	0.173	U_{3c}	L_{1c}
GaSb	0.230	U_{3c}	L_{1c}
InP	0.068	U_{3c}	L_{1c}
InAs	0.226	U_{3c}	L_{1c}
InSb	0.274	U_{3c}	L_{1c}
ZnS	0.342	U_{3c}	X_{1c}
ZnSe	0.074	U_{3c}	X_{1c}
ZnTe	0.063	U_{3c}	L_{1c}
CdS	0.090	U_{3c}	X_{1c}
CdSe	0.120	U_{3c}	L_{1c}
CdTe	0.162	U_{3c}	L_{1c}
HgS	0.294	U_{3c}	L_{1c}
HgSe	0.397	U_{3c}	L_{1c}
HgTe	0.384	U_{3c}	L_{1c}

V. REMARKS

Excellent theoretical works have been carried out to study the stability of the WZ and ZB phases[43] and polytypes.[31,32] Briefly, Yeh *et al.*[43] calculated the total-energy difference between WZ and ZB structures for various semiconductors under the LDA, uncovered a linear scaling between the energy difference and an atomistic orbital-radii coordinate, and exposed chemical trends. Engel and Needs[31] and Cheng, Needs, and Heine[32] calculated the total energies of SiC, ZnS, and Si polytypes, and constructed the theory of polytypism. Therefore, here we will consider only candidate materials for WZ/ZB systems using our calculated total energies of WZ and ZB under the LDA, and those materials which were experimentally observed to have a WZ/ZB structure.

Table IX gives the differences between calculated total energies for WZ and ZB structures of various semicon-

TABLE IX. The difference between the calculated total energies of WZ and ZB structures for various semiconductors. The results of Yeh *et al.* (Ref. 43) and Engel and Needs (Ref. 31) are obtained from figures.

	Difference WZ−ZB (meV/atom)		
Material	Present	Yeh *et al.*	Engel and Needs
C	23.0	25	
Si	6.7	12	7.5
SiC	0.2		4.5
AlN	−18.3	−18	
AlAs	5.3	6	
GaN	−5.1	−9.5	
GaAs	11.7	12.5	
ZnS		3.5	3.3
CdS	−4.4	−2	
CdSe	−1.1		

ductors, together with those from previous theoretical calculations under the LDA. As shown, C, Si, AlAs, and GaAs have a lower total energy for the ZB structure than for the WZ one, while AlN, GaN, and CdS are stable for the WZ structure; both observations are consistent with previous theoretical and experimental results.[43] For SiC and CdSe, however, it is difficult to determine from our calculation which structure is stable, because the difference between the calculated total energies is so small.

Regarding the experimental results, SiC, ZnS, and CdS have many polytypes in nature,[6-8] while Si has WZ/ZB interfaces as stacking faults.[4,5] On the other hand, a single needle crystal of ZnS shows stacking faults and twinning.[9] Recently, Koguchi *et al.*[10] grew GaAs and InAs whiskers, having layered structures comprised of WZ- and ZB-type crystals, by organometallic vapor phase epitaxy. Since the difference in the calculated total energy between the WZ and ZB structures of these semiconductors ranges from -4 to 12 meV/atom, if thermodynamic stability becomes one criterion indicating the existence of WZ/ZB structures, then it is reasonable to suggest that AlAs and CdSe can also grow in WZ/ZB structures under *some* as-yet-unknown growth conditions.

VI. SUMMARY

We have calculated the wurtzite (WZ) and zinc-blende (ZB) band structures of various semiconductors using the first-principles pseudopotential method within the LDA, and then evaluated the band offsets at homomaterial (111) WZ/ZB interfaces for the band-edge states around fundamental gaps. We base our work on the reasonable assumption that there is no difference between the average potential in the WZ and ZB structures. Calculated results were subsequently analyzed using the sp^3-tight-binding method.

Our main results are summarized as follows.

(1) A general tendency exists in the band-gap-character variation (direct or indirect) between the ZB-to-WZ structures: (i) All direct-gap semiconductors in ZB are also direct-gap semiconductors in WZ. (ii) Indirect-gap semiconductors in ZB having an energy level of X_{1c}^{ZB} near L_{1c}^{ZB} or Γ_{1c}^{ZB} are direct-gap semiconductors in WZ, whereas other semiconductors have indirect gaps in both WZ and ZB structures.

(2) A clear one-to-one correspondence is possible between WZ and ZB zone-center states having small wave numbers perpendicular to the [111] direction, and also between the WZ and ZB valence-band states among the zone-boundary states having large wave numbers perpendicular to [111], thereby enabling us to define the band offset at the WZ/ZB interface. On the other hand, although the conduction bands have definite electronic structures, it is difficult to make a correspondence between the conduction-band states among the zone-boundary states in the WZ and ZB structures.

(3) The band offset has a definite sign that is not dependent on the constituent semiconductor materials, but instead on the character of the state. In addition, the WZ/ZB homomaterial systems of C, Si, AlSb, and GaP are of type I, while those of other semiconductors are of type II.

(4) The origin of the band offset is different between the zone-center and zone-boundary states. A difference between the third-nearest-neighboring site in the WZ and ZB structures causes band offsets in the zone-center states, whereas the phase matching of a wave function through the first-nearest-neighboring site causes band offsets in the zone-boundary states. Consequently, the band offsets are larger for the zone-boundary states than for zone-center ones.

(5) The band offsets of the conduction-band states are larger than those of the valence-band states.

(6) A chemical trend appears in which the band offset increases with decreasing ionicity of the constituent semiconductor material, i.e., in the order IV $\geq$ III-V $\geq$ II-VI family compounds. This phenomena is suggested to occur because the magnitude of the band offset is determined by the competition between ionicity and covalency of the constituents.

ACKNOWLEDGMENTS

This work was supported by a Grant-in-Aid from Japan's Ministry of Education, Science and Culture.

APPENDIX: EMPLOYED METHODS FOR THE TIGHT-BINDING ANALYSIS

Here we summarize the Hamiltonian matrices and their eigenenergies used to analyze energy levels in the WZ and ZB structures by the sp^3-tight-binding method. The standard sp^3-atomic-orbital functions were employed as the basis;[54] hence the size of the Hamiltonian matrix for the WZ structure is 16×16,[56] whereas for the ZB one an 8×8 matrix is sufficient. However, in order to clarify the difference between WZ and ZB, we made the unit cell of the ZB structure twice as large (as explained in Sec. II). Thus a matrix of 16×16 elements was applied for both structures.

Figure 7 shows the crystal structure of ZB and WZ

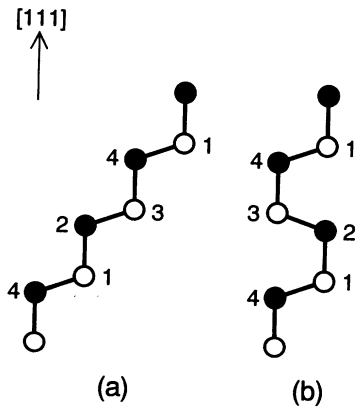

FIG. 7. Schematic diagram of the crystal structures of (a) ZB and (b) WZ along the [111] direction. Only the sites and bonds positioned on the $(1\bar{1}0)$ plane are displayed. Sites are numbered to annotate indexes n and m of submatrices $H(n,m)$ in Eq. (A1).

along the [111] direction, where the atomic sites are numbered as indicated, allowing the Hamiltonian matrix to be divided into 16 submatrices $H(n,m)$, i.e.,

$$H=\begin{bmatrix} H(1,1) & H(1,2) & H(1,3) & H(1,4) \\ H(2,1) & H(2,2) & H(2,3) & H(2,4) \\ H(3,1) & H(3,2) & H(3,3) & H(3,4) \\ H(4,1) & H(4,2) & H(4,3) & H(4,4) \end{bmatrix}, \tag{A1}$$

where each submatrix $H(n,m)$ has elements between the s, p_x, p_y, and p_z Bloch bases of the nth atom, and those of the mth atom.

We adopted the notation of Slater and Koster[57] for the tight-binding parameters. In this approximation, on-site energies are expressed as ε_s^c, ε_s^a, ε_p^c, and ε_p^a, where the superscript c (a) indicates the cation (anion) atom, and s (p) shows the s (p) orbital. Transfer energies are annotated as U, V, and W, which indicate respectively, the transfer energies between the first-, second-, and third-nearest-neighboring sites. $U^{\rm ca}$ and $W^{\rm ca}$ are defined as the transfer energy from cation to anion atoms, while $V^{\rm cc}$ and $V^{\rm aa}$ are defined as that between only cations or anions (see Table VI). The types of transfers ($ss\sigma$, $sp\sigma$, $ps\sigma$, $pp\sigma$, and $pp\pi$) are indicated by subscripts, e.g., $U^{\rm ca}_{ss\sigma}$ and $V^{\rm cc}_{sp\sigma}$.

We considered the Hamiltonian matrices having wave numbers at the $\Gamma^{\rm WZ}$ and $U^{\rm WZ}$ points in the WZ Brillouin zone, and at $\Gamma L^{\rm ZB}$ and $LX^{\rm ZB}$ in the ZB Brillouin zone. The $\Gamma^{\rm WZ}$ and $U^{\rm WZ}$ points have the same wave numbers as the $\Gamma L^{\rm ZB}$ and $LX^{\rm ZB}$ points, respectively. Transfer energies are taken into account from the nearest-neighbor site until a difference appears between the matrices of WZ and ZB. Therefore, at $\Gamma^{\rm WZ}$ and $\Gamma L^{\rm ZB}$, the transfer energy for the first- to third-nearest neighbors is examined, while only the first-nearest one at $U^{\rm WZ}$ and $LX^{\rm ZB}$. In both cases, most submatrices used are in common, and thus only the different submatrices between WZ and ZB are presented here.

The different submatrices between $\Gamma^{\rm WZ}$ and $\Gamma L^{\rm ZB}$ are

$$H^{\rm ZB}(1,2)=\begin{bmatrix} U^{\rm ca}_{ss\sigma} & & & U^{\rm ca}_{sp\sigma} \\ & U^{\rm ca}_{pp\pi} & & \\ & & U^{\rm ca}_{pp\pi} & \\ U^{\rm ca}_{ps\sigma} & & & U^{\rm ca}_{pp\sigma} \end{bmatrix},$$

$$H^{\rm WZ}(1,2)=\begin{bmatrix} U^{\rm ca}_{ss\sigma}+W^{\rm ca}_{ss\sigma} & & & U^{\rm ca}_{sp\sigma}-W^{\rm ca}_{sp\sigma} \\ & U^{\rm ca}_{pp\pi}+W^{\rm ca}_{pp\pi} & & \\ & & U^{\rm ca}_{pp\pi}+W^{\rm ca}_{pp\pi} & \\ U^{\rm ca}_{ps\sigma}-W^{\rm ca}_{ps\sigma} & & & U^{\rm ca}_{pp\sigma}+W^{\rm ca}_{pp\sigma} \end{bmatrix}. \tag{A2}$$

Using Eq. (A2), we obtained energies shown in Eqs. (3) and (4), and

$$E(L^{\rm ZB}_{3v},L^{\rm ZB}_{3c})=\frac{\bar{\varepsilon}^c_p+\bar{\varepsilon}^a_p}{2}\mp\left[\left(\frac{\bar{\varepsilon}^c_p-\bar{\varepsilon}^a_p}{2}\right)^2+(\tfrac{4}{3}U^{\rm ca}_{pp\sigma}+\tfrac{2}{3}U^{\rm ca}_{pp\pi})^2\right]^{1/2},$$
$$E(\Gamma^{\rm WZ}_{5v},\Gamma^{\rm WZ}_{5c})=\frac{\bar{\varepsilon}^c_p+\bar{\varepsilon}^a_p}{2}\mp\left[\left(\frac{\bar{\varepsilon}^c_p-\bar{\varepsilon}^a_p}{2}\right)^2+(\tfrac{4}{3}U^{\rm ca}_{pp\sigma}+\tfrac{2}{3}U^{\rm ca}_{pp\pi}-W^{\rm ca}_{pp\pi})^2\right]^{1/2}, \tag{A3}$$

where the $L^{\rm ZB}_{3v}$ and $\Gamma^{\rm WZ}_{5v}$ ($L^{\rm ZB}_{3c}$ and $\Gamma^{\rm WZ}_{5c}$) states have a negative (positive) sign, $\bar{\varepsilon}^c_p=\varepsilon^c_p+2V^{\rm cc}_{pp\sigma}-2V^{\rm cc}_{pp\pi}$, and $\bar{\varepsilon}^a_p=\varepsilon^a_p+2V^{\rm aa}_{pp\sigma}-2V^{\rm aa}_{pp\pi}$.

On the other hand, the different submatrices between $U^{\rm WZ}$ and $LX^{\rm ZB}$ are

$$H^{\rm ZB}(2,3)=H(1,4)^{\dagger},$$
$$H^{\rm WZ}(2,3)=e^{i2\pi/3}\times W^{\dagger}H^{\rm ZB}(2,3)W, \tag{A4}$$

where submatrix $H(1,4)$ is given by

$$H(1,4)=i\times\begin{bmatrix} U^{\rm ca}_{ss\sigma} & \frac{2\sqrt{6}}{3}U^{\rm ca}_{sp\sigma} & \frac{2\sqrt{2}}{3}U^{\rm ca}_{sp\sigma} & -\frac{1}{3}U^{\rm ca}_{sp\sigma} \\ \frac{2\sqrt{6}}{3}U^{\rm ca}_{ps\sigma} & U^{\rm ca}_{pp\pi} & -\frac{4\sqrt{3}}{9}(U^{\rm ca}_{pp\sigma}-U^{\rm ca}_{pp\pi}) & -\frac{2\sqrt{6}}{9}(U^{\rm ca}_{pp\sigma}-U^{\rm ca}_{pp\pi}) \\ \frac{2\sqrt{2}}{3}U^{\rm ca}_{ps\sigma} & -\frac{4\sqrt{3}}{9}(U^{\rm ca}_{pp\sigma}-U^{\rm ca}_{pp\pi}) & \frac{1}{9}(8U^{\rm ca}_{pp\sigma}+U^{\rm ca}_{pp\pi}) & -\frac{2\sqrt{2}}{9}(U^{\rm ca}_{pp\sigma}-U^{\rm ca}_{pp\pi}) \\ -\frac{1}{3}U^{\rm ca}_{ps\sigma} & -\frac{2\sqrt{6}}{9}(U^{\rm ca}_{pp\sigma}-U^{\rm ca}_{pp\pi}) & -\frac{2\sqrt{2}}{9}(U^{\rm ca}_{pp\sigma}-U^{\rm ca}_{pp\pi}) & \frac{1}{9}(U^{\rm ca}_{pp\sigma}+8U^{\rm ca}_{pp\pi}) \end{bmatrix}, \tag{A5}$$

and we use the diagonal matrices $W_{ij}=w_i\delta_{ij}$, $w_1=w_4=1$, and $w_2=w_3=-1$. The phase factor in Eq. (A4), which emerges due to the different positions of atoms 3 and 4 in the WZ and ZB structures (see Fig. 7), and the existence of Bloch wave vectors perpendicular to [111], causes a difference between the energy spectra of U^{WZ} and LX^{ZB}. Using Eqs. (A4) and (A5), the following energies were analytically obtained in addition to Eqs. (8) and (9):

$$E(X_{5v}^{\mathrm{ZB}},X_{5c}^{\mathrm{ZB}})=\frac{\varepsilon_p^c+\varepsilon_p^a}{2}\mp\left[\left[\frac{\varepsilon_p^c-\varepsilon_p^a}{2}\right]^2+(\tfrac{4}{3}U_{pp\sigma}^{\mathrm{ca}}-\tfrac{4}{3}U_{pp\pi}^{\mathrm{ca}})^2\right]^{1/2},$$
$$E(U_{2v}^{\mathrm{WZ}},U_{2c}^{\mathrm{WZ}})=\frac{\varepsilon_p^c+\varepsilon_p^a}{2}\mp\left[\left[\frac{\varepsilon_p^c-\varepsilon_p^a}{2}\right]^2+|\tfrac{4}{3}e^{i2\pi/3}U_{pp\sigma}^{\mathrm{ca}}-(-1+\tfrac{1}{3}e^{i2\pi/3})U_{pp\pi}^{\mathrm{ca}}|^2\right]^{1/2}. \quad \text{(A6)}$$

[1]See, for example, *Proceedings of the 21st International Conference on the Physics of Semiconductors, Beijing, China, 1992,* edited by P. Jiang and H. Z. Zheng (World Scientific, Singapore, 1992).

[2]M. Murayama and T. Nakayama, J. Phys. Soc. Jpn. **61**, 2419 (1992).

[3]M. Murayama and T. Nakayama, Superlatt. Microstruct. **12**, 215 (1992).

[4]A. Bourret, J. Desseaux, and C. D'Anterroches, in *Microscopy of Semiconducting Materials, 1981, Proceedings of the 2nd Oxford Conference,* edited by A. G. Cullis and D. C. Joy (Institute of Physics, Bristol, 1981), p. 9.

[5]I. G. Salisbury, J. Appl. Phys. **52**, 1108 (1981).

[6]S. Mardix, Phys. Rev. B **33**, 8677 (1986).

[7]J. W. Baars, in *II-VI Semiconducting Compounds 1967 International Conference,* edited by D. G. Thomas (Benjamin, New York, 1967), p. 631.

[8]D. M. Wilcox and D. B. Holt, Thin Solid Films **37**, 109 (1976).

[9]W. L. Garrett, G. Ruban, and F. Williams, J. Phys. Chem. Solids **43**, 497 (1982).

[10]M. Koguchi, H. Kakibayashi, M. Yazawa, K. Hiruma, and T. Katsuyama, Jpn. J. Appl. Phys. **31**, 2061 (1992); M. Yazawa, M. Koguchi, and K. Hiruma, Appl. Phys. Lett. **58**, 1080 (1991); K. Hiruma, T. Katsuyama, K. Ogawa, M. Koguchi, H. Kakibayashi, and G. P. Morgan, *ibid.* **59**, 431 (1991).

[11]T. Ito, Jpn. J. Appl. Phys. **30**, 1349 (1991).

[12]M. A. Khan, R. A. Skogman, J. M. Van Hove, S. Krishnankutty, and R. M. Kolbas, Appl. Phys. Lett. **56**, 1257 (1990); M. Mizuta, S. Fujieda, Y. Matsumoto, and T. Kawamura, Jpn. J. Appl. Phys. **25**, 945 (1986); T. Sasaki and T. Matsuoka, *ibid.* **64**, 4531 (1988); L. C. Kimerling, H. J. Leamy, and J. R. Patel, Appl. Phys. Lett. **30**, 217 (1977); H. Amano, T. Asahi, and I. Akasaki, Jpn. J. Appl. Phys. **29**, 205 (1990).

[13]S. Strite, J. Ruan, Z. Li, A. Salvador, H. Chen, D. J. Smith, W. J. Choyke, and H. Morkoc, J. Vac. Sci. Technol. B **9**, 1924 (1991).

[14]W. A. Harrison, J. Vac. Sci. Technol. **14**, 1016 (1977).

[15]J. Tersoff, Phys. Rev. B **30**, 4874 (1984); J. Tersoff and W. A. Harrison, Phys. Rev. Lett. **58**, 2367 (1987).

[16]M. Cardona and N. E. Christensen, Phys. Rev. B **35**, 6182 (1987).

[17]W. R. L. Lambrecht, B. Segall, and O. K. Andersen, Phys. Rev. B **41**, 2813 (1990).

[18]W. R. L. Lambrecht and B. Segall, Phys. Rev. B **41**, 2832 (1990).

[19]C. G. Van de Walle, Phys. Rev. B **39**, 1871 (1989); **35**, 8154 (1987).

[20]T. Nakayama, J. Phys. Soc. Jpn. **61**, 2434 (1992).

[21]W. E. Pickett, S. G. Louie, and M. L. Cohen, Phys. Rev. B **17**, 815 (1978).

[22]C. G. Van de Walle and R. M. Martin, J. Vac. Sci. Technol. B **4**, 1055 (1986).

[23]M. Y. Chou, M. L. Cohen, and S. G. Louie, Phys. Rev. B **32**, 7979 (1985).

[24]J. L. Birman, Phys. Rev. **115**, 1493 (1959).

[25]M. R. Salehpour and S. Satpathy, Phys. Rev. B **41**, 3048 (1990).

[26]J. D. Joannopoulos and M. L. Cohen, Phys. Rev. B **8**, 2733 (1973); **7**, 2644 (1973).

[27]T. K. Bergstresser and M. L. Cohen, Phys. Rev. **164**, 1069 (1967).

[28]L. F. Mattheiss and J. R. Patel, Phys. Rev. B **23**, 5384 (1981).

[29]J. Sánchez-Dehesa, J. A. Vergés, and C. Tejedor, Phys. Rev. B **24**, 1006 (1981).

[30]M. D. Stiles and D. R. Hamann, Phys. Rev. B **38**, 2021 (1988).

[31]G. E. Engel and R. J. Needs, J. Phys. Condens. Matter **2**, 367 (1990); G. E. Engel, *ibid.* **2**, 6905 (1990); G. E. Engel and R. J. Needs, Phys. Rev. B **41**, 7876 (1990).

[32]C. Cheng, R. J. Needs, and V. Heine, J. Phys. C **21**, 1049 (1988).

[33]*Semiconductors, Physics of Group IV Elements and III-V Compounds,* edited by O. Madelung, Landolt-Börnstein, New Series, Group III, Vol. 17, Pt. a (Springer-Verlag, Berlin, 1982).

[34]*Semiconductors, Physics of II-VI and I-VII Compounds,* edited by O. Madelung, M. Schulz, and H. Weiss, Landolt-Börnstein, New Series, Group III, Vol. 17, Pt. b (Springer-Verlag, Berlin, 1982).

[35]P. Hohenberg and W. Kohn, Phys. Rev. **136**, B864 (1964).

[36]W. Kohn and L. J. Sham, Phys. Rev. **140**, B1133 (1965).

[37]G. B. Bachelet, D. R. Hamann, and M. Schlüter, Phys. Rev. B **26**, 4199 (1982).

[38]D. Ceperley and B. J. Alder, Phys. Lett. **45**, 566 (1980).

[39]J. P. Perdew and A. Zunger, Phys. Rev. B **23**, 5048 (1981).

[40]J. Ihm, A. Zunger, and M. L. Cohen, J. Phys. C **12**, 4404 (1979).

[41]M. T. Yin and M. L. Cohen, Phys. Rev. B **26**, 5668 (1982).

[42]D. J. Chadi and M. L. Cohen, Phys. Rev. B **8**, 5747 (1973).

[43]Chin-Yu Yeh, Z. W. Lu, S. Froyen, and A. Zunger, Phys. Rev. B **45**, 12 130 (1992), and references therein.

[44]M. S. Hybertsen and S. G. Louie, Phys. Rev. Lett. **55**, 1418 (1985); Phys. Rev. B **32**, 7005 (1985); **34**, 5390 (1986).

[45]R. W. Godby, M. Schlüter, and L. J. Sham, Phys. Rev. Lett. **56**, 2415 (1986); Phys. Rev. B **37**, 10 159 (1988).

[46]B. Zhang, D. Tomanek, S. G. Louie, M. L. Cohen, and M. S. Hybertsen, Solid State Commun. **66**, 585 (1988).

[47]M. S. Hybertsen and M. Schlüter, Phys. Rev. B **36**, 9683 (1987).

[48]J. P. Perdew and M. Levy, Phys. Rev. Lett. **51**, 1884 (1983).

[49]L. J. Sham and M. Schlüter, Phys. Rev. Lett. **51**, 1888 (1983).

[50]G. P. Das, P. Blöchl, O. K. Andersen, N. E. Christensen, and O. Gunnarsson, Phys. Rev. Lett. **63**, 1168 (1989).

[51]R. W. Godby, L. J. Sham, and M. Schlüter, Phys. Rev. Lett. **65**, 2083 (1990).
[52]S.-H. Wei and A. Zunger, referred to in J. E. Bernard and A. Zunger, Phys. Rev. B **36**, 3199 (1987).
[53]E. R. Weber and H. Alexander, J. Phys. Paris (Colloq.) **44**, C4-319 (1983).
[54]P. Vogl, H. P. Hjalmarson, and J. D. Dow, J. Phys. Chem. Solids **44**, 365 (1983).
[55]D. J. Chadi, Phys. Rev. B **16**, 790 (1977).
[56]A. Kobayashi, O. F. Sankey, S. M. Volz, and J. D. Dow, Phys. Rev. B **28**, 935 (1983).
[57]C. Slater and G. F. Koster, Phys. Rev. **94**, 1498 (1954).

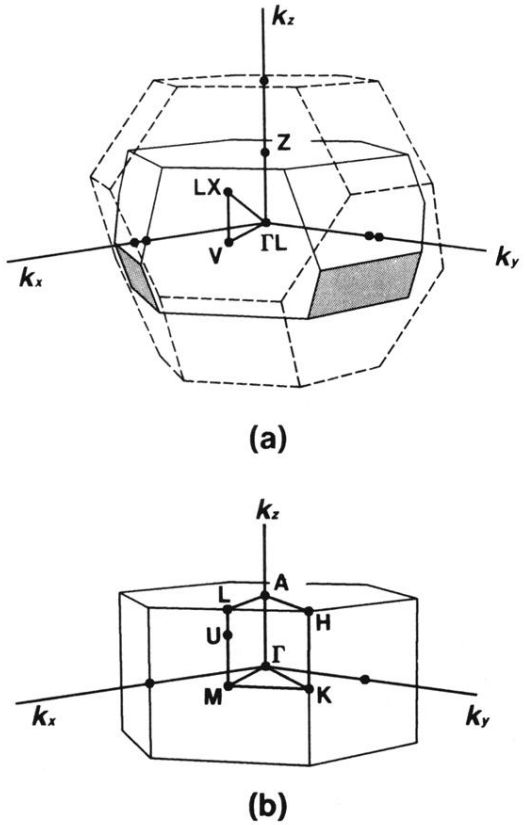

FIG. 1. Brillouin zones for (a) ZB and (b) WZ structures. Both Brillouin zones are drawn in the same scale and viewed from the same point, where the k_z axis is parallel to the [111] direction. In (a), the broken line indicates the familiar fcc Brillouin zone, the solid line that of the $\frac{1}{2}$ Brillouin zone corresponding to the double unit cell along the [111] direction. V is located at the center of the front surface of the $\frac{1}{2}$ Brillouin zone, and LX is located at the center of the hexagon of the fcc Brillouin zone, whose position is inside of the $\frac{1}{2}$ Brillouin zone and just above V along the [111] direction. The shaded planes indicate the surface common to both Brillouin zones. In (b), U divides the L-M line at a 1:2 ratio.